PLB-985 neutrophil-like cells release antifungal extracellular vesicles against the human-pathogenic fungus *Aspergillus fumigatus*

Muhammad Rafiq[a,#], Flora Rivieccio[a,b,#], Ann-Kathrin Zimmermann[a,b,#], Corissa Visser[a,b], Alexander Bruch[c], Thomas Krüger[a], Katherine González[a,b], Olaf Kniemeyer[a,b], Matthew G. Blango[c], Axel A. Brakhage[a,b]*

[a] Department of Molecular and Applied Microbiology, Leibniz Institute for Natural Product Research and Infection Biology - Hans Knöll Institute (Leibniz-HKI), Jena, Germany.

[b] Department of Microbiology and Molecular Biology, Institute of Microbiology, Friedrich Schiller University, Jena, Germany.

[c] Junior Research Group RNA Biology of Fungal Infections, Leibniz Institute for Natural Product Research and Infection Biology - Hans Knöll Institute (Leibniz-HKI), Jena, Germany.

Running Title: Neutrophil-like model of *A. fumigatus* infection

Key Words: *Aspergillus fumigatus*, PLB-985, phagocytosis, fungal pathogens, extracellular vesicles, HL-60

*Correspondence: E-mail axel.brakhage@leibniz-hki.de

Tel. +49 (0)3641-532 1001.

# These authors contributed equally to the manuscript and were listed alphabetically

ABSTRACT

Fungal infections remain a major global concern. Emerging fungal pathogens and increasing rates of resistance mean that additional research efforts and resources must be allocated to advancing our understanding of fungal pathogenesis and developing new therapeutic interventions. Neutrophilic granulocytes are a major cell type involved in protection against the important fungal pathogen *Aspergillus fumigatus*, where they employ numerous defense mechanisms, including production of antimicrobial extracellular vesicles. A major draw-back to work with neutrophils is the lack of a suitable cell line system for the study of fungal pathogenesis. To address this problem, we assessed the feasibility of using differentiated PLB-985 neutrophil-like cells as an in vitro model to study *A. fumigatus* infection. We find that dimethylformamide-differentiated PLB-985 cells provide a useful recapitulation of many aspects of *A. fumigatus* interactions with primary human polymorphonuclear leukocytes. We find that differentiated PLB-985 cells phagocytose fungal conidia and acidify conidia-containing phagolysosomes similar to primary neutrophils, release neutrophil extracellular traps, and also produce antifungal extracellular vesicles in response to infection. In addition, we provide an improved method for the isolation of extracellular vesicles produced during infection by employing a size-exclusion chromatography-based approach. Advanced LC-MS/MS proteomics revealed an enrichment of extracellular vesicle marker proteins and a decrease of cytoplasmic proteins in extracellular vesicles isolated using this improved method. Ultimately, we find that differentiated PLB-985 cells can serve as a genetically tractable model to study many aspects of *A. fumigatus* pathogenesis.

IMPORTANCE

Polymorphonuclear leukocytes are an important defense against human fungal pathogens, yet our model systems to study this group of cells remains very limited in scope. In this study, we established that differentiated PLB-985 cells can serve as a model to recapitulate several important aspects of human polymorphonuclear leukocyte interactions with the important human fungal pathogen *Aspergillus fumigatus*. The proposed addition of a cultured neutrophil-like cell line to the experimental toolbox to study fungal pathogenesis will allow for a more mechanistic description of neutrophil antifungal biology. In addition, the easier handling of the cell line compared to primary human neutrophils allowed us to use PLB-985 cells to provide an improved method for isolation of neutrophil-derived extracellular vesicles using size-exclusion chromatography. Together, these results provide significant tools and a baseline knowledge for the future study of neutrophil-derived extracellular vesicles in the laboratory.

INTRODUCTION

Fungal infections remain a tremendous source of global morbidity and mortality. More than 1 billion individuals are affected by fungal infections per year, with invasive infections killing numbers comparable to other leading bacterial pathogens (>1.5 million per year; gaffi.org; (1)). Deadly invasive infections are caused by a relatively small number of fungi, with most of these attributed to members of the genera *Candida*, *Pneumocystis*, *Cryptococcus*, and *Aspergillus* (2). *Aspergillus fumigatus* causes most of the fungal infections by the *Aspergilli* and is particularly dangerous to immunocompromised individuals suffering from neutropenia (3). There is also emerging evidence to suggest that invasive aspergillosis may contribute to COVID-19-related deaths (4, 5), but challenges in safely obtaining bronchoalveolar lavage samples from these patients have often made confirmatory diagnosis difficult and unsafe. Despite the obvious importance of *A. fumigatus* in the clinic, our understanding of this important pathogen remains lacking in many aspects, in part due to a lack of tractable experimental systems in the laboratory.

Mammals are continuously challenged by fungal pathogens. In fact, asexual spores of *A. fumigatus*, termed conidia, are thought to be inhaled by humans on a scale of hundreds per day (6). For most fungi, the body temperature of mammals is too high to allow for growth, but for organisms like *A. fumigatus* that thrive in compost piles at high temperatures, the human host provides fertile ground in the absence of a functional immune system (7). However, humans do have multiple additional defenses, including a mucociliary escalator to remove particles from the lungs, a robust epithelium, aggressive alveolar macrophages that remove the majority of the remaining fungal conidia, and infiltrating polymorphonuclear leukocytes (PMNs) that aid in clearance of conidia and destruction of fungal hyphae, among others (3, 8). Neutrophils play an essential role in antifungal defense, due to their importance in killing fungal hyphae. This is well-illustrated by the high susceptibility of neutropenic patients to *A. fumigatus* infections in the clinics (reviewed in (3)).

Studies in primary human neutrophils have revealed the capacity of these cells to phagocytose conidia and release granules, neutrophil extracellular traps (NETs), and extracellular vesicles in response to invading pathogens (9-11). Phagocytosis occurs in conjunction with recognition of pathogen-associated molecular patterns by host pathogen recognition receptors. In neutrophils and macrophages, internalized wild-type *A. fumigatus* conidia are capable of stalling phagolysosomal acidification to facilitate outgrowth (12). Studies in zebrafish and mice have shown that these internalized conidia can even be passed from neutrophils to macrophages for destruction of the fungus (13), further implying complex intracellular trafficking.

In addition to phagocytosis, NETs are an important mechanism of defense against *A. fumigatus* that are produced in response to fungal recognition in a CD11b-dependent manner (10, 14). NET production is most abundant against hyphae, but NETs are also sometimes produced in response to resting and swollen conidia (15). In vivo, NETs were shown to be present in mouse lungs during infection but were generally dispensable for fungal

clearance (15, 16), suggesting that alternative measures are required to eliminate fungal hyphae that escaped phagocytosis as conidia.

Extracellular vesicles serve as an additional antifungal mechanism against *A. fumigatus* hyphae and conidia (9). Antifungal extracellular vesicles produced by neutrophils in response to infection are capable of associating with the fungal cell wall and are in some cases internalized to deliver an unknown antifungal cargo. Intriguingly, the antifungal effect of these extracellular vesicles appeared to be tailored to the infecting pathogen, as spontaneously released vesicles and vesicles released in response to a knockout strain deficient in production of the conidial pigment dihydroxynaphthalene (DHN)-melanin were not antifungal against wild-type fungus. The dissection of the molecular mechanisms behind these differences in antifungal potential are difficult to discern in the absence of a tractable model system for the genetic manipulation of neutrophils. Despite the importance of neutrophils in antifungal defense, the majority of studies are still performed in primary human PMNs isolated from venous blood, a resource that can only be used for small-scale studies and is unfortunately highly variable between blood donors. A laborious isolation procedure and limited half-life of about 19 hours ex vivo (17) also make more mechanistic studies difficult. For all these reasons, establishment of a cell culture line to study *A. fumigatus* pathogenesis in neutrophils or neutrophil-like cells would be highly advantageous. In recent years some options have emerged to investigate specific aspects of neutrophil biology in culture (18). In particular, the myeloid cell line PLB-985, a derivative of HL-60 granulocytic cells, has recently emerged as a tractable model to study NET formation in response to bacterial infection after differentiation into neutrophil-like cells (19, 20). Of note, the related HL-60 cell line has also been used previously to deliver azole drugs to *A. fumigatus*-infected mice (21), but not to our knowledge in studies of *A. fumigatus* pathogenesis.

In this study we hypothesized that differentiated human PLB-985 neutrophil-like cells could serve as model system to study the host-pathogenesis of *A. fumigatus* in a blood donor-independent manner. We tested this hypothesis by defining the phagocytosis and intracellular trafficking of *A. fumigatus* conidia by PLB-985 cells, the production of neutrophil extracellular traps, and the production of extracellular vesicles produced in response to fungal infection. We find numerous similarities between primary neutrophils and PLB-985 cells that suggest differentiated PLB-985 cells can serve as a tractable in vitro model system for further study of some aspects of *A. fumigatus* pathogenesis.

RESULTS

Differentiated PLB-985 neutrophil-like cells phagocytose opsonized *A. fumigatus* conidia.

We set out to assess the feasibility of using dimethylformamide (DMF)-differentiated PLB-985 (dPLB) cells as a model for neutrophil phagocytosis, NET production, and extracellular vesicle release. Upon infection, neutrophils

are known to rapidly phagocytose and process *A. fumigatus* conidia. We therefore challenged dPLB cells with opsonized *A. fumigatus* resting conidia and assessed phagocytosis by confocal laser scanning microscopy and imaging flow cytometry. We began by measuring induction of cell damage following infection using lactate dehydrogenase (LDH) release assays and found that LDH levels were below the limit of detection for dPLB cells after 2 and 4 hours of incubation (data not shown). We observed that dPLB cells were able to phagocytose fluorescein isothiocyanate (FITC)-labelled conidia (green), as evidenced by a phagosomal membrane surrounding the conidia (**Fig. 1A).** To measure phagocytosis, we analyzed 5,000 host cells post-infection by single-cell analysis using imaging flow cytometry. For this we counterstained with calcofluor white (CFW; blue) to elucidate non-phagocytosed conidia (**Fig. 1B and Fig. S1A to B**). Further quantification of imaging flow cytometry data revealed that approximately 20% of wild-type and 25% of non-pigmented *ΔpksP* conidia were phagocytosed by dPLBs after 2 hours, while undifferentiated PLB-985 cells exhibited limited phagocytosis (**Fig. 1C**). To determine if infection also resulted in an activated immune response, we measured proinflammatory cytokine levels by enzyme-linked immunosorbent assay (ELISA). Infection of dPLB cells with wild-type opsonized resting spores resulted in production of slightly increased levels of interleukin (IL)-8, but not IL-1β after 6 hours of infection (**Fig. 1D**). Basal levels of IL-1β were relatively high in untreated dPLBs and primary human PMNs compared to values in the literature (22), suggesting some basal activation; however, levels of IL-8 appeared similar to expected. In comparison, PMNs secreted low amounts of IL-1β independent of the presence of fungal conidia, while the level of IL-8 increased only slightly after infection (**Fig. S1C**). Based on these results, we chose to proceed with differentiated PLB-985 cells for the remainder of the study.

Internalized *A. fumigatus* conidia are processed inside dPLB phagolysosomes.

Following internalization of conidia by professional phagocytes like macrophages and neutrophils, conidia-containing phagosomes fuse with lysosomes to acidify the compartment and aid in fungal killing. Numerous additional enzymes are activated upon phagolysosomal acidification to degrade and digest the internalized fungal conidia. The acidification and maturation of phagolysosomes are regulated by protein complexes assembled on the phagolysosomal membrane, including lysosomal-associated membrane protein (LAMP)-1, 2, and 3; several vacuolar ATPases (V-ATPases); Ras-related protein (RAB) 5 and 7; Flotillin 1 and 2; and numerous others (23). DHN-melanin on the surface of conidia can interfere with these processes in alveolar macrophages, monocytes, and primary neutrophils to delay fungal processing and phagolysosomal acidification (12). To test whether dPLB cells process conidia similarly to primary human PMNs, we first stained the cells with LAMP-1, a general endocytic marker on the membrane of phagolysosomes. LAMP-1 showed a clear signal around phagolysosomes of infected cells (**Fig. 2A**), and the intensity of the signal did not differ between wild-type and *ΔpksP* conidia (**Fig. 2B**).

Furthermore, loading dPLB cell with Lysotracker, a weak base that becomes fluorescent under acidic conditions, showed that the *ΔpksP* conidia-containing phagosomes were significantly more acidified than those containing wild-type conidia, revealing that DHN-melanin can also block the acidification process in the dPLB model as well (**Fig. 2C to D**).

The interference of the acidification pathway in alveolar macrophages by fungal DHN-melanin occurs through the inhibition of V-ATPase assembly (24, 25). This multiprotein complex plays a major role in lowering the pH from 6 to <4.5 by pumping H^+ ions across the phagolysosomal membrane. Staining of the V-ATPase V1 subunit in dPLB cells revealed that the percentage of recruitment to conidia-containing phagolysosomes was similar for wild-type and *ΔpksP* conidia (**Fig. S2A to B**), suggesting that other proton pumps may contribute to acidification of the phagolysosomes in neutrophil-like cells.

A. fumigatus triggers formation of NETs from dPLB cells.

One defense mechanism employed by neutrophilic granulocytes to fight against pathogens is the formation of NETs. These structures consist of condensed chromatin and various enzymes that are released into the extracellular space and typically correlate with death of the cell (26). NETs contain several anti-fungal proteins, which are responsible for the fungistatic effect against *A. fumigatus* hyphae (15). To test if dPLBs are also able to form NETs in response to *A. fumigatus* and serve as a model for this pathway, we co-incubated dPLBs cells with hyphae and stained for nucleic acid with 4',6-diamidino-2-phenylindole (DAPI; **Fig. 3A**). As a positive control, we activated NET formation using phorbol myristate acetate, a known trigger of NET formation in PLB-985 cells (**Fig. 3B**; (19, 27)). We observed the presence of histone H3 embedded in the DNA fibers and an association of NETs with fungal hyphae (**Fig. 3B**). Taken together these results showed that *A. fumigatus* is able to trigger NET formation in dPLB cells and that these NETs are specifically directed against the hyphae.

dPLB cells produce extracellular vesicles in response to infection.

Recently, a new defense mechanism from neutrophilic granulocytes was discovered, the production of antimicrobial extracellular vesicles (28, 29). These small lipid-enclosed nanoparticles are released from primary PMNs after contact with microorganisms and, in the case of *A. fumigatus* conidia, can inhibit fungal growth after coincubation (9). This effect is likely due in part to their protein cargo, which consists of antimicrobial peptides such as azurocidin and cathepsin G. To assess if dPLB cells can produce extracellular vesicles spontaneously or in response to *A. fumigatus*, we incubated cells with or without conidia for 2 and 4 h. Next, we isolated extracellular vesicles using two different methods; first using a previously described differential centrifugation-based approach (DC; (9)) that enriches for small and medium-sized extracellular vesicles and a second approach that relies on size-

exclusion chromatography (SEC) to purify a more selective population of smaller extracellular vesicles. Using these methods, dPLB cells were observed to actively secrete extracellular vesicles over time in a manner comparable to primary human PMNs (**Fig. 4A to B**). Using nanoparticle tracking analysis, we observed the median size of particles to be around 200 nm, comparable to extracellular vesicles derived from primary neutrophils, a feature that was comparable between infection-derived and spontaneously released extracellular vesicles (**Fig. 4C to D**).

We next compared the protein content of dPLB-derived extracellular vesicles isolated using each isolation method with and without fungal infection by LC-MS/MS-based proteomics analysis. We were able to identify 1,984 unique proteins across all four samples (**Dataset S1**). The majority of identified proteins (737 proteins) were found in all four samples (**Fig. 5A**). We expected that isolation using size-exclusion chromatography would improve the quality of the isolated particles as has been shown previously (30), and this was in fact the case. We observed an increase in extracellular vesicle markers like the tetraspanins CD63 and CD81, and tumor susceptibility gene 101 (TSG101), and a decrease in cytoplasmic proteins like calnexin (CANX; **Table 1**). These results again suggest that isolation using size-exclusion chromatography further enriches for extracellular vesicles over differential centrifugation alone.

Extracellular vesicles produced by primary PMNs in response to *A. fumigatus* infection are known to be enriched for antimicrobial cargo proteins like azurocidin, cathepsin G, and defensin (9). In line, we found that dPLBs also contained many of these same proteins in both infection-derived and spontaneously released extracellular vesicles (**Table 1**), with some notable exceptions. For example, dPLBs appeared to lack defensin, neutrophil elastase, and some histone proteins previously observed. In addition, we noticed minimal changes between spontaneously released extracellular vesicles and infection-derived extracellular vesicles using both isolation methods (**Fig. 5A and Dataset S1**). In fact, this seems to confirm our findings with cytokine measurements above, suggesting that DMF-based differentiation of PLB cells induces a basal level of activation that is reflected in the extracellular vesicle population. We also observed an enrichment for serum proteins like immunoglobulins and complement factors in our infection-derived samples (**Fig. 5B to C and Table S1**). These proteins are likely introduced during the opsonization of fungal conidia prior to infection, and potentially represent a contamination of soluble proteins in our preparations, despite thorough washing of opsonized spores. It remains formally possible that these serum factors are incorporated into, or bound externally, to extracellular vesicles upon infection. Interestingly, we see relatively similar abundances of serum proteins between spontaneously released and infection-derived vesicles using each isolation method, but we did observe an enrichment for serum factors in the size-exclusion chromatography-based approach over the differential centrifugation strategy. Ultimately, the extracellular vesicles produced by dPLB cells in response to infection by *A. fumigatus* appear to be similar to those produced by human PMNs in previous reports as evidenced by an

Upset plot showing overlapping proteins cohorts (**Fig. S3;** (9)). Improvements in LC-MS/MS technology and the advantage of higher input amounts of extracellular vesicle protein using large amounts of dPLB cells in culture resulted in significantly more proteins detected in the dataset provided here compared to efforts using primary neutrophils (9). Ultimately, dPLBs offer a scalable system for the elucidation of novel mechanisms of neutrophil extracellular vesicle biology.

dPLB extracellular vesicles produced against *A. fumigatus* limit fungal growth.

The most compelling feature of infection-derived extracellular vesicles of human neutrophils is likely their antifungal capacity, as we previously reported (9). We set out to determine if the extracellular vesicles produced by dPLB cells in response to *A. fumigatus* opsonized conidia are antifungal to a mitochondrial-GFP reporter strain used previously as a marker of fungal viability (31). Extracellular vesicles isolated using differential centrifugation in a manner comparable to previous reports (9) proved to be antifungal to the mitochondrial-GFP reporter strain. This was evidenced by fragmentation of fungal mitochondria after administration of extracellular vesicles to conidia that were allowed to germinate for 6 hours prior to overnight incubation with extracellular vesicles, 3 mM H_2O_2 as a positive control, or left untreated as a negative control (**Fig. 6**). Four representative images are shown to indicate the spectrum of phenotypes observed for each experimental condition. These results suggest a comparable effect for infection-derived extracellular vesicles on *A. fumigatus* hyphae to those reported previously for primary human PMNs (9) and make dPLB cells an ideal tool to understand underlying mechanisms of extracellular vesicle biology during infection.

MATERIALS AND METHODS

Fungal strains cultivation and opsonization.

Cultivation of *A. fumigatus* strains CEA10 (Fungal Genetics Stock Center; A1163), CEA17 Δ*akuB*^{ku80} Δ*pksP* (32), and AfS35/pJW103 (31) was performed on malt agar plates (Sigma-Aldrich) supplemented to a final concentration of 2% (wt/vol) agar for 5 days at 37 °C. Conidia were harvested in sterile, ultra-distilled water, filtered through a 30 µm-pore filter (MACS, Miltenyi Biotec) and counted with a Thoma chamber. Prior to confrontation with PLB-985 cells, conidia were opsonized with normal human serum (Merck Millipore). Briefly, 900 µl of spore suspension was mixed with 100 µl of normal human serum and incubated in a thermomixer at 37 °C for 30 min shaking at 500 rpm. The spore suspension was washed three times by collecting spores *via* centrifugation at 1800 x *g* for 1 min at 4 °C and resuspending in fresh PBS 1X. Following washing, spores were enumerated in a Thoma chamber in preparation for infection assays.

Cell culture cultivation, differentiation, and infection.

PLB-985 cells were maintained in Roswell Park Memorial Institute medium 1640 (RPMI; Gibco) supplemented with 10% (vol/vol) fetal bovine serum (FBS; HyClone, GE Life science), 100 U/ml penicillin-streptomycin antibiotic solution (Lonza, Switzerland) and 2 mM UltraGlutamine (alanyl L-glutamine; Gibco). For differentiation into a neutrophilic granulocyte cell type, 4×10^5 cells/ml were resuspended in supplemented RPMI medium containing 2.5% (vol/vol) FBS and 0.5% DMF (Sigma-Aldrich) for 4 days at 37 °C with 5% (vol/vol) CO_2. On day 4, fresh differentiation medium was added, and the cells were incubated for 3 additional days. On day 7, cells were collected, centrifuged at 1200 x *g* for 5 min and then seeded in wells for experiments at the appropriate concentrations noted in the text. The medium used for all the assays was composed of RPMI supplemented with 1% (vol/vol) exosome-depleted FBS (Life Technologies GmbH), 2 mM UltraGlutamine, and 0.5% (vol/vol) DMF.

Determination of cell viability.

To assess cell viability after confrontation with *A. fumigatus* conidia, the release of LDH was determined using the CyQUANT™ LDH cytotoxicity assay kit (Thermo Fisher Scientific, UK) according to the manufacturer´s instruction. Cells treated with *A. fumigatus* conidia with a multiplicity of infection (MOI) of 5 for 2 h were tested for their LDH activity, which was compared to the spontaneous LDH activity and the maximum LDH activity. Release of LDH was not detected in three independent biological replicates.

Immunofluorescence assays.

For immunofluorescence, cells were allowed to adhere in a 24-well plate with poly-L-lysine-coated glass coverslips (Merck). After infection with *A. fumigatus*-labelled spores and incubation for the noted times, cells were fixed using 3.7% (vol/vol) formaldehyde for 10 min, rinsed three times with PBS 1X, permeabilized for 15 min using 0.1% (vol/vol) Triton X-100 in PBS or 0.1% (vol/vol) saponin in PBS, and blocked for 30 min with 2% (wt/vol) bovine serum albumin (BSA). After permeabilization, washed cells were incubated with primary rabbit anti-Lamp-1 antibody (Abcam 24170, 1:100 dilution), anti-V-ATPase V1 subunit antibody (Abcam 73404, 1:100 dilution), or anti-Histone H3 (Cell signaling DIH2, 1:200 dilution) antibody in 1% (wt/vol) BSA in PBS, followed by incubation with secondary goat anti-rabbit IgG antibody DyLight 633 (Thermo Fisher Scientific). Lastly, the glass cover slips were mounted onto microscopy slides and visualized using Zeiss LSM 780 confocal microscope (Carl Zeiss). LAMP-1 recruitment was quantified by comparing the positive signal from stained phagolysosomes to non-stained phagolysosomes.

Acidification assays.

Acidification assays were performed as mentioned previously (25). Briefly, the cells were incubated with 50 nM lysotracker DND-99 (Thermo Fisher Scientific) for one hour prior to infection. After that, FITC-labeled conidia were added to the cells for 2 or 4 hours and imaged using a Zeiss LSM 740 (Carl-Zeiss, Germany). For quantification, two hundred conidia-containing phagolysosomes were counted and evaluated for acidification. The values represent the mean ± SD of three separate experiments.

Cytokine measurement.

For the detection of IL-8 and IL-1β, $2x10^5$ dPLB cells were seeded in 1 mL of assay medium in a 24 well plate. After addition of conidia at a MOI of 5, plates were incubated at 37 °C + 5% (vol/vol) CO_2 for 2, 4, or 6 hours. As a positive control, cells were treated with 5 µg/mL of lipopolysaccharide (LPS; Sigma-Aldrich L4516). At the appropriate end point, samples were collected, spun down at 300 x *g* for 5 min to remove cell debris, and frozen at -20 °C for a maximum of 3 days. Cytokines were measured using human ELISA Max deluxe kits (BioLegend) according to the manufacturer´s instruction.

Extracellular vesicle isolation.

After infection with *A. fumigatus* the supernatant of dPLB cells was collected, and extracellular vesicles were isolated using two different methods: a differential centrifugation-based approach or a size exclusion chromatography-based approach. The first method was described previously for the isolation of neutrophil-derived extracellular vesicles (9, 28). In both approaches, samples were centrifuged at 3000 x *g* for 15 min at 4 °C and then filtered through 5-µm pore size filters (Carl Roth). In the first method, samples were then centrifuged at 19,500 x *g* for 30 min at 4 °C to collect small- to medium-sized extracellular vesicles. For the second approach, the clarified filtrate was concentrated using Amicon Ultra-15 centrifugal filters (Merck) with a molecular mass cut-off (MWCO) of 100 kDa for 10 min at 4 °C and 4000 *x g* and finally loaded on size-exclusion chromatography qEV 70 nm columns (Izon). After discarding the 3 mL void volume, 1.5 mL of extracellular vesicle sample were collected and measured. When necessary, extracellular vesicles were further concentrated using 10 kDa cutoff Amicon Ultra-0.5 ml filters (Merck, Germany). Extracellular vesicles were used fresh, without freezing, for all downstream experiments.

Nanoparticle tracking analysis.

Particle concentration and size distribution were analyzed using a nanoparticle tracking analysis (NTA) NS300 device with a 650 nm laser (Malvern Instruments Ltd., UK). Samples were measured with a constant flow rate of 20 and a temperature set to 25 °C. Five 60 second videos were recorded with a camera level of 11 for dPLB and of

9 for primary neutrophils extracellular vesicles. Videos were then analyzed with the NTA 3.2.16 software using a detection threshold of 4.

Phagocytosis assays.

To assess the phagocytic ability of PLB-985 differentiated and un-differentiated cells, we used a combination of imaging flow cytometry and confocal fluorescence microscopy. For both methods the conidia were first stained with fluorescein isothiocyanate (FITC) and then after confrontation of PLB-985 cells, counterstained with calcofluor white (CFW; Sigma -Aldrich). The FITC solution was obtained by dissolving FITC powder (Sigma-Aldrich) in 5 mL of 0.1 M sodium carbonate Na_2CO_3 followed by filtration through a 0.22-µm pore size filter (Carl Roth). Afterwards 1 ml of this solution was mixed with 500 µl of spore suspension and incubated for 30 min at 37 °C with 1000 rpm in the dark. The spores were then pelleted and washed three times with PBS with 0.001% (vol/vol) Tween 20 (Carl Roth). During the last washing step Tween was removed to avoid residual detergent in the samples (12, 33). Before counting, the conidia were opsonized following the protocol described above. They were then added to the cells and co-incubated for 2 and 4 h at 37 °C with 5% (vol/vol) CO_2. At the end of each time point, 1 µg/ml of CFW was added and incubated for 1 min. Afterwards the cell suspension was transferred to microcentrifuge tubes, centrifuged at 600 x *g* for 2 min at 4 °C and washed with PBS twice. After discarding the supernatant, the pellet was fixed with 150 µL of 3.7% (vol/vol) formaldehyde in PBS at room temperature for 15 min and subsequently washed again as described above. For imaging flow cytometry measurements, the cells were then resuspended in 150 µL of PBS and analyzed immediately or stored at 4 °C for no more than 24 h. Three independent experiments were performed and for each replicate 5000 cells were analyzed using the ImageStream X Mark II (Luminex). A 488 nm laser was used to detect FITC staining and a 405 nm laser for the CFW. The laser voltage was adjusted to the conidia strain. For WT conidia, we used 10 mW of 488 nm laser and 2 mW for the 405 nm laser, and for Δ*pksP* 1 and 2 mW of the respective lasers. The fluorescence intensities of the samples were compensated and analyzed with the IDEAS software (Luminex), an example of the gating strategy used for analysis can be found in the supplement files (**Fig. S1B**). For the fluorescence microscopy analysis, cells were spotted on a microscopy slide after fixation and visualized using a Zeiss LSM 5 Live (Carl Zeiss, Jena, Germany) microscope from at least three biological replicates as described above.

Protein preparation for LC-MS/MS.

After isolation as described above, extracellular vesicles were delipidated as described previously (9) using the protein precipitation protocol of Wessel and Flügge (34). Delipidated extracellular vesicles were resolubilized in 100 µl of 50 mM triethyl ammonium bicarbonate (TEAB) in 1:1 (v/v) trifluoroethanol/water. For reduction of

cysteine thiols, the solution was mixed with 10 mM Tris(2-carboxyethyl) phosphine and alkylated with 12.5 mM chloroacetamide at 70 °C for 30 min in the dark. Proteins were digested for 18 h at 37 °C with trypsin/LysC mix (Promega) at a protein-to-protease ratio of 25:1. Tryptic peptides were first completely evaporated using a vacuum concentrator (Eppendorf) and then resolubilized in 0.05% trifluoroacetic acid (TFA) in 2:98 (v/v) acetonitrile/water. Finally, the samples were filtered through Ultrafree-MC Hydrophilic PTFE membrane (0.2 µm pore size) spin filters (Millipore) and stored at -20 °C until measurement. Each sample was measured in triplicate (3 analytical replicates of 3 biological replicates) as follows.

LC-MS/MS analysis.

LC-MS/MS analysis was performed on an Ultimate 3000 nano RSLC system connected to a QExactive HF mass spectrometer (both Thermo Fisher Scientific). Peptide trapping for 5 min on an Acclaim Pep Map 100 column (2 cm x 75 µm, 3 µm) at 5 µL/min was followed by separation on an analytical Acclaim Pep Map RSLC nano column (50 cm x 75 µm, 2µm). Mobile phase gradient elution of eluent A (0.1% (v/v) formic acid in water) mixed with eluent B (0.1% (v/v) formic acid in 90/10 acetonitrile/water) was performed as follows: 0 min at 4% B, 30 min at 12% B, 75 min at 30% B, 85 min at 50% B, 90-95 min at 96% B, 95.1-120 min at 4% B.

Positively charged ions were generated at spray voltage of 2.2 kV using a stainless-steel emitter attached to the Nanospray Flex Ion Source (Thermo Fisher Scientific). The quadrupole/orbitrap instrument was operated in Full MS / data dependent MS2 (Top15) mode. Precursor ions were monitored at m/z 300-1500 at a resolution of 120,000 FWHM (full width at half maximum) using a maximum injection time (ITmax) of 120 ms and an AGC (automatic gain control) target of $3 \cdot 10^6$. Precursor ions with a charge state of z=2-5 were filtered at an isolation width of m/z 1.6 amu for further HCD fragmentation at 27% normalized collision energy (NCE). MS2 ions were scanned at 15,000 FWHM (ITmax=100 ms, AGC= $2 \cdot 10^5$). Dynamic exclusion of precursor ions was set to 25 s and the underfill ratio was set to 1.0%. The LC-MS/MS instrument was controlled by Chromeleon 7.2, QExactive HF Tune 2.8 and Xcalibur 4.0 software.

Database search and data analysis

Tandem mass spectra were searched against the UniProt database of *Homo sapiens* (https://www.uniprot.org/proteomes/UP000005640; 2021/05/17) and *Neosartorya fumigata* (https://www.uniprot.org/proteomes/UP000002530; 2021/05/17) using Proteome Discoverer (PD) 2.4 (Thermo) and the algorithms of Mascot 2.4.1 (Matrix Science, UK), Sequest HT (version of PD2.2), MS Amanda 2.0, and MS Fragger 3.2. Two missed cleavages were allowed for the tryptic digestion. The precursor mass tolerance was set to 10 ppm and the fragment mass tolerance was set to 0.02 Da. Modifications were defined as dynamic Met

oxidation, and protein N-term acetylation with and without methionine-loss as well as static Cys carbamidomethylation. A strict false discovery rate (FDR) < 1% (peptide and protein level) were required for positive protein hits. If only 1 peptide per protein has been identified the hit was accepted if the Mascot score was >30 or the MS Amanda score was >300 or the Sequest score was >4 or the MS Fragger score was >8. The Percolator node of PD2.4 and a reverse decoy database was used for qvalue validation of spectral matches. Only rank 1 proteins and peptides of the top scored proteins were counted. Label-free protein quantification was based on the Minora algorithm of PD2.2 using a signal-to-noise ratio >5. Imputation of missing quan values was applied by setting the abundance to 75% of the lowest abundance identified for each sample. Normalization was based on a replicate median total peptide sum approach, which was calculated based on the sum of all identified peptide abundance values per replicate sample. The sums of each of the three replicates from the four sample groups were used to calculate median values. Normalization factors were calculated by dividing median values of the respective sample group by the abundance sum of each sample. Normalization factors were multiplied with single protein abundance values of each replicate/sample. The p-values are based on a Student`s t-test. Ratio-adjusted p-values were calculated by dividing p-values with the log4ratio of the protein abundance levels. Significant differences in protein abundance were defined when the following three requirements were reached: At least a 4-fold change in abundance (up and down), a ratio-adjusted p-value <0.05, and at least identified in 2 of 3 replicates of the sample group with the highest abundance. Intersection plots were created using the UpSetR package (35) and only include proteins that were detected in at least two replicates of a given sample. Volcano plots were created using ggplot2 in R using the replicate median total peptide sum normalized (RMN) data for all proteins detected in **Dataset S1**.

Fungal mitochondrial reporter inhibition assay

To characterize growth inhibition and killing of hyphae by fungal-induced extracellular vesicles an *A. fumigatus* strain expressing a mitochondrial GFP reporter (AfS35/pJW103; (31)) has been used as described previously (9). extracellular vesicles produced by $1x10^7$ dPLB have been isolated and co-incubated with the reporter strain. After 16 h of incubation samples were stained with CFW and images were taken using confocal fluorescence microscopy (Zeiss LSM 5 Live; Carl Zeiss, Germany).

Data availability

The mass spectrometry proteomics data have been deposited to the ProteomeXchange Consortium via the PRIDE partner repository (36) with the dataset identifier PXD027032.

Statistical Analysis. Data were plotted and statistically analyzed using GraphPad Prism software 5.0 (GraphPad Software) unless otherwise noted. The Student's t test was used for significance testing when comparing two groups. Differences between the groups were considered significant at a P value of <0.05. Throughout the article, significance is denoted as follows: *, P = <0.05; **, P = <0.01, ***, P = <0.001; ns, nonsignificant.

Ethics Statement. Peripheral human blood was collected from healthy volunteers only after written informed consent was provided. The study was conducted in accordance with the Declaration of Helsinki and approved by the Ethics Committee of the University Hospital Jena (permit number 273-12/09).

DISCUSSION

Neutrophils are critical in the immune response to fungal pathogens like *A. fumigatus* in the lung, as evidenced by the high fungal burden in neutropenic mouse models and the abundance of invasive aspergillosis cases in patients lacking neutrophilic granulocytes (37-39). The importance of neutrophils stems from their numerous antimicrobial capacities, including the ability to phagocytose pathogens, degranulate, produce reactive oxygen species, form NETs, and release extracellular vesicles (9, 40). Previous studies with *A. fumigatus* and human PMNs have mostly focused on understanding NET production, reactive oxygen species generation, and phagocytosis, including the mechanisms that lead to internalization and activation of an antifungal response (41, 42). Numerous cell lines have been considered to model neutrophils in vitro, with limited success. The most promising remains the HL-60 leukemia cell line and PLB-985 sublineage, which have even been used as a model for aspergillosis and bacterial killing (19-21). Following differentiation these cells have been shown to exhibit some common features of primary neutrophils. We therefore hypothesized that DMF-differentiated PLB-985 myeloid cells could serve as a model for several aspects of the neutrophil immune response to *A. fumigatus* infection.

Primary neutrophils are capable of phagocytosing and processing *A. fumigatus* conidia, a feature that was maintained in dPLB cells. A mutant strain (Δ*pksP*) lacking the DHN-melanin layer on the surface of conidia was phagocytosed more efficiently than the wild-type strain, in agreement with all the published data showing the protective role of DHN-melanin against immune cells (43). The observed phagocytosis rate was similar to primary neutrophils, which internalized around 40% of wild-type conidia after 2 h, reaching a maximum of 50% after 4 or 12 h (44, 45). Measuring the release of inflammatory cytokines from dPLBs revealed that IL-8, but not IL-1β, increased over time following infection with opsonized conidia. These results are consistent with those collected from primary PMNs co-incubated with L-ficolin opsonized conidia for 8 h, where secretion of IL-8 was also much higher than IL-1β (46). Notably, the basal levels of cytokine release were above the expected baseline, suggesting that differentiation with DMF may result in partial activation of PLB-985 cells. Differentiation method will

436 therefore remain an important consideration for researchers trying to sensitively measure cytokine increases in
437 response to fungal stimuli.

438 We also stained the cells for the endosomal marker LAMP-1 and measured the acidification of the
439 phagolysosomes via Lysotracker. These experiments confirmed that around 20% of wild-type conidia are
440 completely internalized inside the phagosomes and that lysosomal fusion occurs as a next step of conidial
441 processing. Interestingly, and as already demonstrated for primary monocytes and neutrophils (12), melanized
442 conidia showed less acidification around the phagolysosomal membrane than the mutant lacking DHN melanin.
443 This effect in monocytes is caused by inhibition of V-ATPase assembly. Surprisingly, staining for the V1 subunit of
444 the V-ATPase did not reveal a significant difference between the wild-type and Δ*pksP* strains in dPLB cells as has
445 been observed in other cell systems. These results suggest that neutrophils likely employ additional mechanisms
446 to acidify phagolysosomes in neutrophilic granulocytes after *A. fumigatus* infection. Together, these results
447 suggest that dPLBs can serve as an intriguing model to study various aspects of neutrophil phagocytosis and
448 intracellular processing in a more tractable in vitro model system.

449 Human lungs are frequently confronted with airborne fungal pathogens like *A. fumigatus*. In the healthy
450 lung, professional phagocytes and the mucociliary escalator rapidly remove conidia, but in immunocompromised
451 patients, conidia can initiate germination and form hyphae. The hyphal morphotype is much more difficult to
452 eliminate and requires the antifungal activity of neutrophils. One mechanism that aids in control of *A. fumigatus*
453 hyphae is the release of fungistatic NETs composed of DNA and antimicrobial proteins; however, their fungistatic
454 activity is known to be low (10, 15, 47). By staining for extracellular DNA and NET constituent histone H3, we could
455 clearly show that dPLB cells also produce NETs in response to *A. fumigatus* hyphae, comparable to primary human
456 PMNs and in agreement with other studies challenging dPLBs with bacterial pathogens (19, 20). As we expected
457 from previous reports (20), dPLB cells serve as an appropriate model for NET production in response to *A.*
458 *fumigatus* infection.

459 Production of extracellular vesicles from primary neutrophils co-incubated with *Aspergillus* conidia or
460 bacteria like *Staphylococcus aureus* is an important defense strategy against microorganisms (9, 28). The small
461 size and low abundance of host-derived extracellular vesicles means that collection of these particles from
462 infection systems remains challenging. In the case of primary human PMNs, large amounts of blood from donors
463 are needed to perform experiments. We were therefore highly motivated to assess the extracellular vesicles
464 produced by dPLB cells as a potential supplemental approach for isolation of vesicles from primary cells. We found
465 that dPLB cells were also able to generate comparable populations of extracellular vesicles to PMNs upon contact
466 with opsonized conidia. Secretion of extracellular vesicles of approximately 200 nm in diameter increased over
467 time, independently of the isolation method we applied. Proteomic analysis revealed that by using a size-exclusion

chromatography-based isolation approach, the extracellular vesicles population could be enriched for extracellular vesicle marker proteins like CD63, CD81, and TSG101. We observed that the samples obtained by this method had a higher abundance of proteins and showed more differences between the spontaneously released and infection-derived extracellular vesicles. In particular, infection-derived extracellular vesicles were enriched in immunoglobulins and complement factors compared to spontaneously released vesicles. It is likely that these serum proteins are introduced to the infection system during opsonization of the fungal conidia, despite thorough washing. It remains unclear whether these immunoglobulins and complement factors play an important role in extracellular vesicle biology during *A. fumigatus* infection or are instead just a protein contaminant detected by the very sensitive LC-MS/MS technique. As a hint that immunoglobulins may play an important role in extracellular vesicle biology during infection, the association of immunoglobulins and complement proteins was shown previously to be important in systemic lupus erythematosus (SLE) disease, where extracellular vesicles with immunoglobulin cargo could act as immune complexes to mediate inflammation (48, 49).

In the proteomic analysis of extracellular vesicles derived from primary neutrophils infected with *A. fumigatus*, several antimicrobial peptides, such as cathepsin G and azurocidin, were detected (9). Co-incubation of the extracellular vesicles from primary neutrophils with fungal hyphae arrested growth. Using dPLB cells, we also identified extracellular vesicles containing cathepsin G and azurocidin; however, the distribution remained relatively equal between spontaneously released and infection-derived extracellular vesicles. We suspect that this is due to a low level of activation of the dPLB cells during the differentiation with DMF. Nevertheless, we performed co-incubation experiments with extracellular vesicles and fungal hyphae to test their ability to inhibit fungal growth and observed inhibition with infection-derived but not spontaneously released extracellular vesicles. We can postulate several reasons for this somewhat confounding result. First, it is possible that immunoglobulins are playing a more specific role and are required to target the extracellular vesicles effectively to the fungal hyphae. In this case, the protein cargo may be the same, but targeting would be inefficient in spontaneously released extracellular vesicles. Against this argumentation, the opsonization of the bacterial pathogen *Staphylococcus aureus* was not found to influence the antimicrobial capacity of neutrophil-derived extracellular vesicles. A second option is that additional extracellular vesicle cargo molecules such as RNA or lipids may play a role in the antifungal activity. It has been shown in many instances now that extracellular vesicles can contain small RNAs that exert distinct functions during infection, especially in regard to plant fungal pathogens (50, 51). For this reason, we believe that a combination of factors are likely involved in the antifungal effect of extracellular vesicles.

In conclusion our results suggest that DMF-differentiated PLB-985 cells can be used as a model to study certain aspects of the interaction of the human pathogenic fungus *A. fumigatus* with neutrophilic granulocytes.

Although, they will never substitute for all experiments with neutrophils, we do believe that this system will serve as a useful tool for the genetic dissection of some essential aspects of *A. fumigatus* pathogenesis.

ACKNOWLEDGEMENTS

We would like to thank Johannes Wagener for providing the *A. fumigatus* mito-GFP strain. The work presented here was generously supported by the Deutsche Forschungsgemeinschaft (DFG)-funded Collaborative Research Center/Transregio FungiNet 124 'Pathogenic fungi and their human host: Networks of Interaction' (210879364, project A1 and Z2), the DFG-funded ANR project AfuInf, and by the Federal Ministry for Education and Research (BMBF: https://www.bmbf.de/), Germany, Project FKZ 01K12012 "RFIN – RNA-Biologie von Pilzinfektionen." The authors declare no conflicts of interest.

REFERENCES

1. Brown GD, Denning DW, Gow NA, Levitz SM, Netea MG, White TC. 2012. Hidden killers: human fungal infections. Sci Transl Med 4:165rv13.
2. Schmiedel Y, Zimmerli S. 2016. Common invasive fungal diseases: an overview of invasive candidiasis, aspergillosis, cryptococcosis, and Pneumocystis pneumonia. Swiss Med Wkly 146:w14281.
3. Latge JP, Chamilos G. 2019. *Aspergillus fumigatus* and Aspergillosis in 2019. Clin Microbiol Rev 33.
4. Nasir N, Farooqi J, Mahmood SF, Jabeen K. 2020. COVID-19-associated pulmonary aspergillosis (CAPA) in patients admitted with severe COVID-19 pneumonia: An observational study from Pakistan. Mycoses 63:766-770.
5. Salmanton-Garcia J, Sprute R, Stemler J, Bartoletti M, Dupont D, Valerio M, Garcia-Vidal C, Falces-Romero I, Machado M, de la Villa S, Schroeder M, Hoyo I, Hanses F, Ferreira-Paim K, Giacobbe DR, Meis JF, Gangneux JP, Rodriguez-Guardado A, Antinori S, Sal E, Malaj X, Seidel D, Cornely OA, Koehler P, FungiScope European Confederation of Medical Mycology/The International Society for H, Animal Mycology Working G. 2021. COVID-19-Associated Pulmonary Aspergillosis, March-August 2020. Emerg Infect Dis 27:1077-1086.
6. Rivera A, Hohl TM, Collins N, Leiner I, Gallegos A, Saijo S, Coward JW, Iwakura Y, Pamer EG. 2011. Dectin-1 diversifies *Aspergillus fumigatus*-specific T cell responses by inhibiting T helper type 1 CD4 T cell differentiation. J Exp Med 208:369-81.
7. Brakhage AA, Langfelder K. 2002. Menacing mold: the molecular biology of *Aspergillus fumigatus*. Annu Rev Microbiol 56:433-55.
8. Drummond RA, Gaffen SL, Hise AG, Brown GD. 2014. Innate Defense against Fungal Pathogens. Cold Spring Harb Perspect Med 5.
9. Shopova IA, Belyaev I, Dasari P, Jahreis S, Stroe MC, Cseresnyes Z, Zimmermann AK, Medyukhina A, Svensson CM, Kruger T, Szeifert V, Nietzsche S, Conrad T, Blango MG, Kniemeyer O, von Lilienfeld-Toal M, Zipfel PF, Ligeti E, Figge MT, Brakhage AA. 2020. Human Neutrophils Produce Antifungal Extracellular Vesicles against *Aspergillus fumigatus*. mBio 11.
10. McCormick A, Heesemann L, Wagener J, Marcos V, Hartl D, Loeffler J, Heesemann J, Ebel F. 2010. NETs formed by human neutrophils inhibit growth of the pathogenic mold *Aspergillus fumigatus*. Microbes Infect 12:928-36.
11. Brogan TD. 1964. Effect of Complement and of the Carbohydrate Components of Sputum on Phagocytosis by Human Polymorphonuclear Leucocytes. Immunology 7:626-38.

12. Thywissen A, Heinekamp T, Dahse HM, Schmaler-Ripcke J, Nietzsche S, Zipfel PF, Brakhage AA. 2011. Conidial Dihydroxynaphthalene Melanin of the Human Pathogenic Fungus *Aspergillus fumigatus* Interferes with the Host Endocytosis Pathway. Front Microbiol 2:96.
13. Pazhakh V, Ellett F, Croker BA, O'Donnell JA, Pase L, Schulze KE, Greulich RS, Gupta A, Reyes-Aldasoro CC, Andrianopoulos A, Lieschke GJ. 2019. beta-glucan-dependent shuttling of conidia from neutrophils to macrophages occurs during fungal infection establishment. PLoS Biol 17:e3000113.
14. Silva JC, Rodrigues NC, Thompson-Souza GA, Muniz VS, Neves JS, Figueiredo RT. 2020. Mac-1 triggers neutrophil DNA extracellular trap formation to *Aspergillus fumigatus* independently of PAD4 histone citrullination. J Leukoc Biol 107:69-83.
15. Bruns S, Kniemeyer O, Hasenberg M, Aimanianda V, Nietzsche S, Thywissen A, Jeron A, Latge JP, Brakhage AA, Gunzer M. 2010. Production of extracellular traps against *Aspergillus fumigatus* in vitro and in infected lung tissue is dependent on invading neutrophils and influenced by hydrophobin RodA. PLoS Pathog 6:e1000873.
16. Clark HL, Abbondante S, Minns MS, Greenberg EN, Sun Y, Pearlman E. 2018. Protein Deiminase 4 and CR3 Regulate *Aspergillus fumigatus* and beta-Glucan-Induced Neutrophil Extracellular Trap Formation, but Hyphal Killing Is Dependent Only on CR3. Front Immunol 9:1182.
17. Lahoz-Beneytez J, Elemans M, Zhang Y, Ahmed R, Salam A, Block M, Niederalt C, Asquith B, Macallan D. 2016. Human neutrophil kinetics: modeling of stable isotope labeling data supports short blood neutrophil half-lives. Blood 127:3431-8.
18. Blanter M, Gouwy M, Struyf S. 2021. Studying Neutrophil Function in vitro: Cell Models and Environmental Factors. J Inflamm Res 14:141-162.
19. Marin-Esteban V, Turbica I, Dufour G, Semiramoth N, Gleizes A, Gorges R, Beau I, Servin AL, Lievin-Le Moal V, Sandre C, Chollet-Martin S. 2012. Afa/Dr diffusely adhering *Escherichia coli* strain C1845 induces neutrophil extracellular traps that kill bacteria and damage human enterocyte-like cells. Infect Immun 80:1891-9.
20. Amulic B, Knackstedt SL, Abu Abed U, Deigendesch N, Harbort CJ, Caffrey BE, Brinkmann V, Heppner FL, Hinds PW, Zychlinsky A. 2017. Cell-Cycle Proteins Control Production of Neutrophil Extracellular Traps. Developmental Cell 43:449-462.e5.
21. Baistrocchi SR, Lee MJ, Lehoux M, Ralph B, Snarr BD, Robitaille R, Sheppard DC. 2017. Posaconazole-Loaded Leukocytes as a Novel Treatment Strategy Targeting Invasive Pulmonary Aspergillosis. J Infect Dis 215:1734-1741.
22. Iula L, Keitelman IA, Sabbione F, Fuentes F, Guzman M, Galletti JG, Gerber PP, Ostrowski M, Geffner JR, Jancic CC, Trevani AS. 2018. Autophagy Mediates Interleukin-1β Secretion in Human Neutrophils. Front Immunol 9:269.
23. Goyette G, Boulais J, Carruthers NJ, Landry CR, Jutras I, Duclos S, Dermine JF, Michnick SW, LaBoissiere S, Lajoie G, Barreiro L, Thibault P, Desjardins M. 2012. Proteomic characterization of phagosomal membrane microdomains during phagolysosome biogenesis and evolution. Mol Cell Proteomics 11:1365-77.
24. Heinekamp T, Schmidt H, Lapp K, Pahtz V, Shopova I, Koster-Eiserfunke N, Kruger T, Kniemeyer O, Brakhage AA. 2015. Interference of *Aspergillus fumigatus* with the immune response. Semin Immunopathol 37:141-52.
25. Schmidt F, Thywissen A, Goldmann M, Cunha C, Cseresnyes Z, Schmidt H, Rafiq M, Galiani S, Graler MH, Chamilos G, Lacerda JF, Campos A, Jr., Eggeling C, Figge MT, Heinekamp T, Filler SG, Carvalho A, Brakhage AA. 2020. Flotillin-Dependent Membrane Microdomains Are Required for Functional Phagolysosomes against Fungal Infections. Cell Rep 32:108017.
26. Branzk N, Papayannopoulos V. 2013. Molecular mechanisms regulating NETosis in infection and disease. Semin Immunopathol 35:513-30.
27. Xie K, Varatnitskaya M, Maghnouj A, Bader V, Winklhofer KF, Hahn S, Leichert LI. 2020. Activation leads to a significant shift in the intracellular redox homeostasis of neutrophil-like cells. Redox Biol 28:101344.

28. Timar CI, Lorincz AM, Csepanyi-Komi R, Valyi-Nagy A, Nagy G, Buzas EI, Ivanyi Z, Kittel A, Powell DW, McLeish KR, Ligeti E. 2013. Antibacterial effect of microvesicles released from human neutrophilic granulocytes. Blood 121:510-8.
29. Brakhage AA, K. ZA, Rivieccio F, Visser C, Blango MG. 2021. Host-derived extracellular vesicles for antimicrobial defense. microLife doi:10.1093/femsml/uqab003/6228840.
30. Lane RE, Korbie D, Trau M, Hill MM. 2019. Optimizing Size Exclusion Chromatography for Extracellular Vesicle Enrichment and Proteomic Analysis from Clinically Relevant Samples. Proteomics 19:e1800156.
31. Ruf D, Brantl V, Wagener J. 2018. Mitochondrial Fragmentation in *Aspergillus fumigatus* as Early Marker of Granulocyte Killing Activity. Front Cell Infect Microbiol 8:128.
32. Hillmann F, Novohradska S, Mattern DJ, Forberger T, Heinekamp T, Westermann M, Winckler T, Brakhage AA. 2015. Virulence determinants of the human pathogenic fungus *Aspergillus fumigatus* protect against soil amoeba predation. Environ Microbiol 17:2858-69.
33. Kraibooj K, Schoeler H, Svensson CM, Brakhage AA, Figge MT. 2015. Automated quantification of the phagocytosis of *Aspergillus fumigatus* conidia by a novel image analysis algorithm. Front Microbiol 6:549.
34. Wessel D, Flugge UI. 1984. A method for the quantitative recovery of protein in dilute solution in the presence of detergents and lipids. Anal Biochem 138:141-3.
35. Lex A, Gehlenborg N, Strobelt H, Vuillemot R, Pfister H. 2014. UpSet: Visualization of Intersecting Sets. IEEE Trans Vis Comput Graph 20:1983-92.
36. Perez-Riverol Y, Xu QW, Wang R, Uszkoreit J, Griss J, Sanchez A, Reisinger F, Csordas A, Ternent T, Del-Toro N, Dianes JA, Eisenacher M, Hermjakob H, Vizcaino JA. 2016. PRIDE Inspector Toolsuite: Moving Toward a Universal Visualization Tool for Proteomics Data Standard Formats and Quality Assessment of ProteomeXchange Datasets. Mol Cell Proteomics 15:305-17.
37. Stephens-Romero SD, Mednick AJ, Feldmesser M. 2005. The pathogenesis of fatal outcome in murine pulmonary aspergillosis depends on the neutrophil depletion strategy. Infect Immun 73:114-25.
38. Muhlemann K, Wenger C, Zenhausern R, Tauber MG. 2005. Risk factors for invasive aspergillosis in neutropenic patients with hematologic malignancies. Leukemia 19:545-50.
39. King J, Henriet SSV, Warris A. 2016. Aspergillosis in Chronic Granulomatous Disease. J Fungi (Basel) 2.
40. Feldmesser M. 2006. Role of neutrophils in invasive aspergillosis. Infect Immun 74:6514-6.
41. Cunha C, Kurzai O, Loffler J, Aversa F, Romani L, Carvalho A. 2014. Neutrophil responses to aspergillosis: new roles for old players. Mycopathologia 178:387-93.
42. Braem SG, Rooijakkers SH, van Kessel KP, de Cock H, Wosten HA, van Strijp JA, Haas PJ. 2015. Effective Neutrophil Phagocytosis of Aspergillus fumigatus Is Mediated by Classical Pathway Complement Activation. J Innate Immun 7:364-74.
43. Heinekamp T, Thywissen A, Macheleidt J, Keller S, Valiante V, Brakhage AA. 2012. *Aspergillus fumigatus* melanins: interference with the host endocytosis pathway and impact on virulence. Front Microbiol 3:440.
44. Hartung S, Rauh C, Hoang TNM, Jahreis S, Wagner K, Macheleidt J, Brakhage AA, Rummler S, Hochhaus A, von Lilienfeld-Toal M. 2019. Fast and Quantitative Evaluation of Human Leukocyte Interaction with *Aspergillus fumigatus* Conidia by Flow Cytometry. Cytometry A 95:332-338.
45. Shepardson KM, Jhingran A, Caffrey A, Obar JJ, Suratt BT, Berwin BL, Hohl TM, Cramer RA. 2014. Myeloid derived hypoxia inducible factor 1-alpha is required for protection against pulmonary *Aspergillus fumigatus* infection. PLoS Pathog 10:e1004378.
46. Bidula S, Sexton DW, Schelenz S. 2016. Serum opsonin ficolin-A enhances host-fungal interactions and modulates cytokine expression from human monocyte-derived macrophages and neutrophils following *Aspergillus fumigatus* challenge. Med Microbiol Immunol 205:133-42.
47. Gazendam RP, van Hamme JL, Tool AT, Hoogenboezem M, van den Berg JM, Prins JM, Vitkov L, van de Veerdonk FL, van den Berg TK, Roos D, Kuijpers TW. 2016. Human Neutrophils Use Different Mechanisms To Kill *Aspergillus fumigatus* Conidia and Hyphae: Evidence from Phagocyte Defects. J Immunol 196:1272-83.

638 48. Buzas EI, Toth EA, Sodar BW, Szabo-Taylor KE. 2018. Molecular interactions at the surface of extracellular
639 vesicles. Semin Immunopathol 40:453-464.
640 49. Perez-Hernandez J, Redon J, Cortes R. 2017. Extracellular Vesicles as Therapeutic Agents in Systemic Lupus
641 Erythematosus. Int J Mol Sci 18.
642 50. Cai Q, Qiao L, Wang M, He B, Lin FM, Palmquist J, Huang SD, Jin H. 2018. Plants send small RNAs in
643 extracellular vesicles to fungal pathogen to silence virulence genes. Science 360:1126-1129.
644 51. He B, Cai Q, Qiao L, Huang C-Y, Wang S, Miao W, Ha T, Wang Y, Jin H. 2021. RNA-binding proteins
645 contribute to small RNA loading in plant extracellular vesicles. Nature Plants doi:10.1038/s41477-021-
646 00863-8.

647

648

649 **FIGURES**

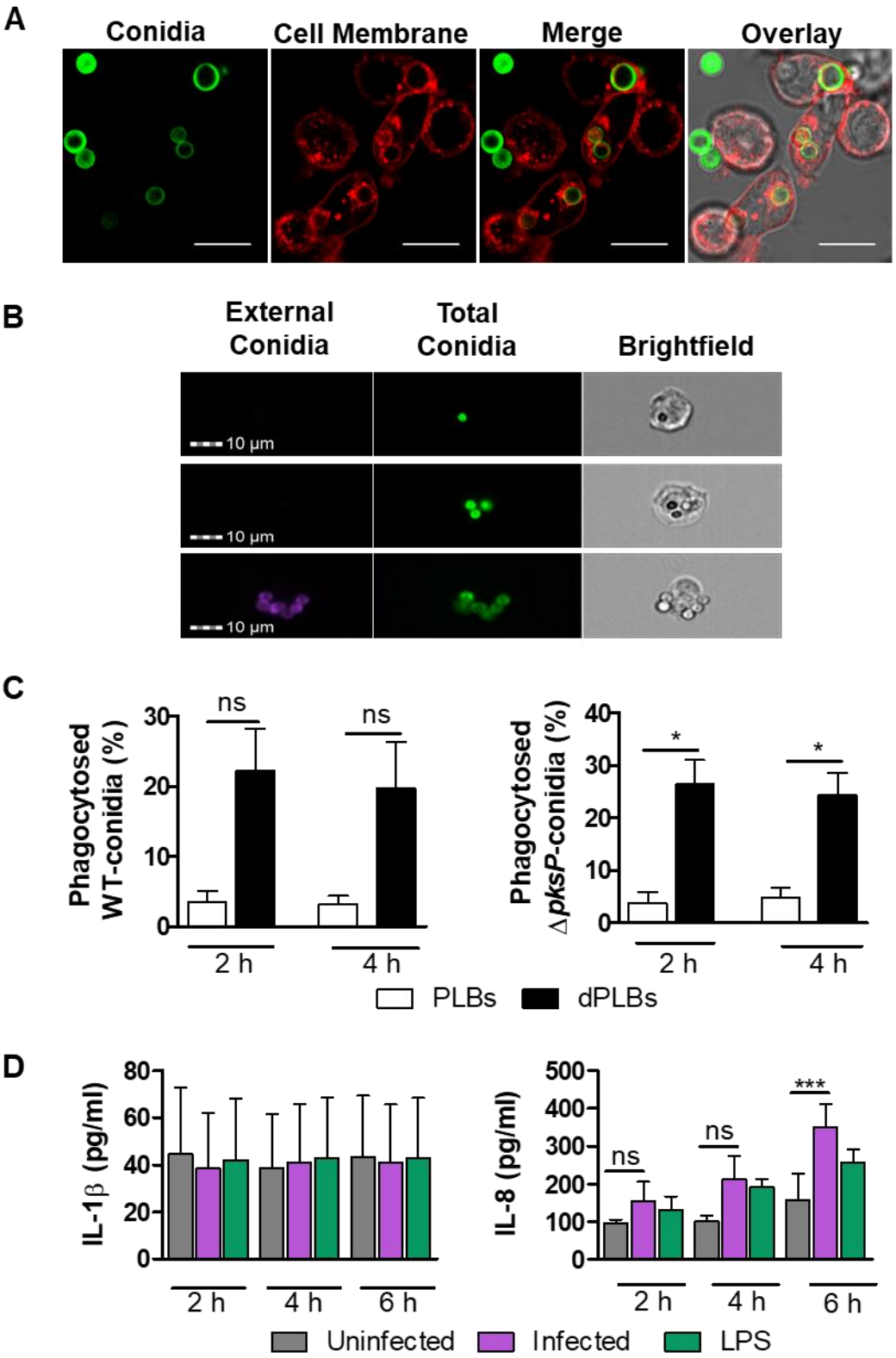

650

651 **FIG 1. Phagocytosis of *A. fumigatus* conidia by PLB-985 cells.**

652 **(A)**. Confocal microscopy images of wild-type conidia (FITC-stained; green) phagocytosed by dPLB cells after 4 h
653 co-incubation. Membranes were stained with Cell Mask (red). Images are representative of three independent
654 biological experiments. Scale bars are 10 µm. **(B)** Representative images of wild-type FITC-stained conidia
655 phagocytosed by dPLB cells after 4 h co-infection obtained by imaging flow cytometry (top two rows). External
656 conidia are visualized by counter staining with CFW (purple), as seen in the bottom row. Images are
657 representative of three independent experiments. **(C)** Quantification of phagocytosis using the IDEAs software
658 on 5,000 cells per condition with either wild-type or Δ*pksP* conidia from three independent experiments **(D)**
659 ELISA detection of cytokines IL-1β and IL-8 released from infected dPLBs at different time points.
660 Lipopolysaccharide (LPS) was included for comparison of a bacterial stimulus. Data are presented as mean ±SD,
661 from six biological replicates; * = $p < 0.05$.
662

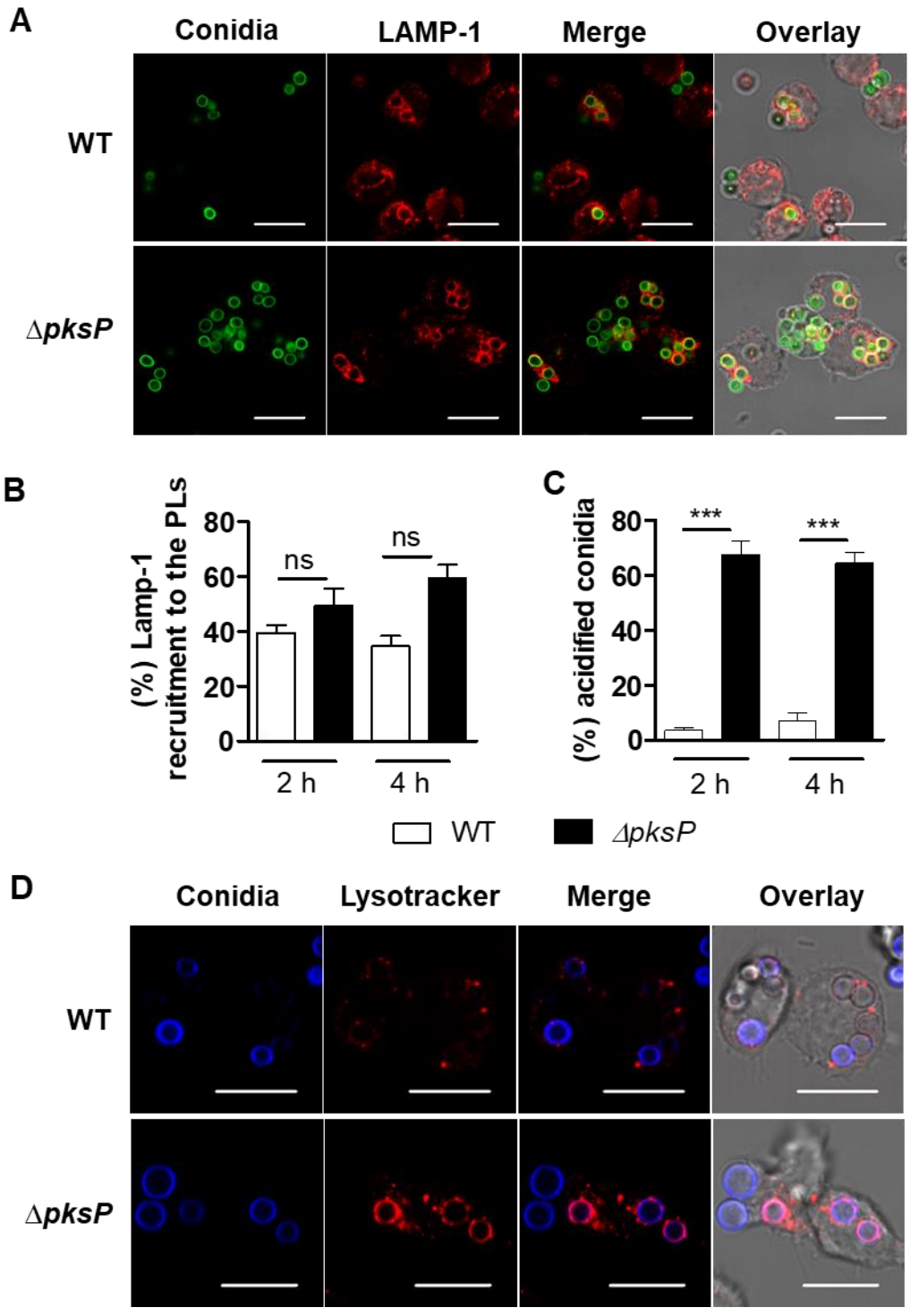

FIG 2. Processing of *A. fumigatus* conidia inside phagolysosomes.

(A) dPLB cells were stained with LAMP-1 (red) after infection with wild-type or Δ*pksP* conidia (FITC labeled; green) for 4 h. Images are representative of three biological replicates. Scale bars are 10 µm. **(B)** Quantification of LAMP-1 co-localization with CFW-labelled conidia in phagolysosomes and **(C)** percentage of acidified conidia

668 in dPLB cells after 2 and 4 h post-infection with wild-type and Δ*pksP* conidia. Data are presented as mean ±SD;
669 *** = $p < 0.001$. **(D)** Colocalization of conidia (CFW; blue) in acidified compartments labeled with Lysotracker
670 (red). Images are representative of three biological replicates. Scale bars are 10 µm.
671
672

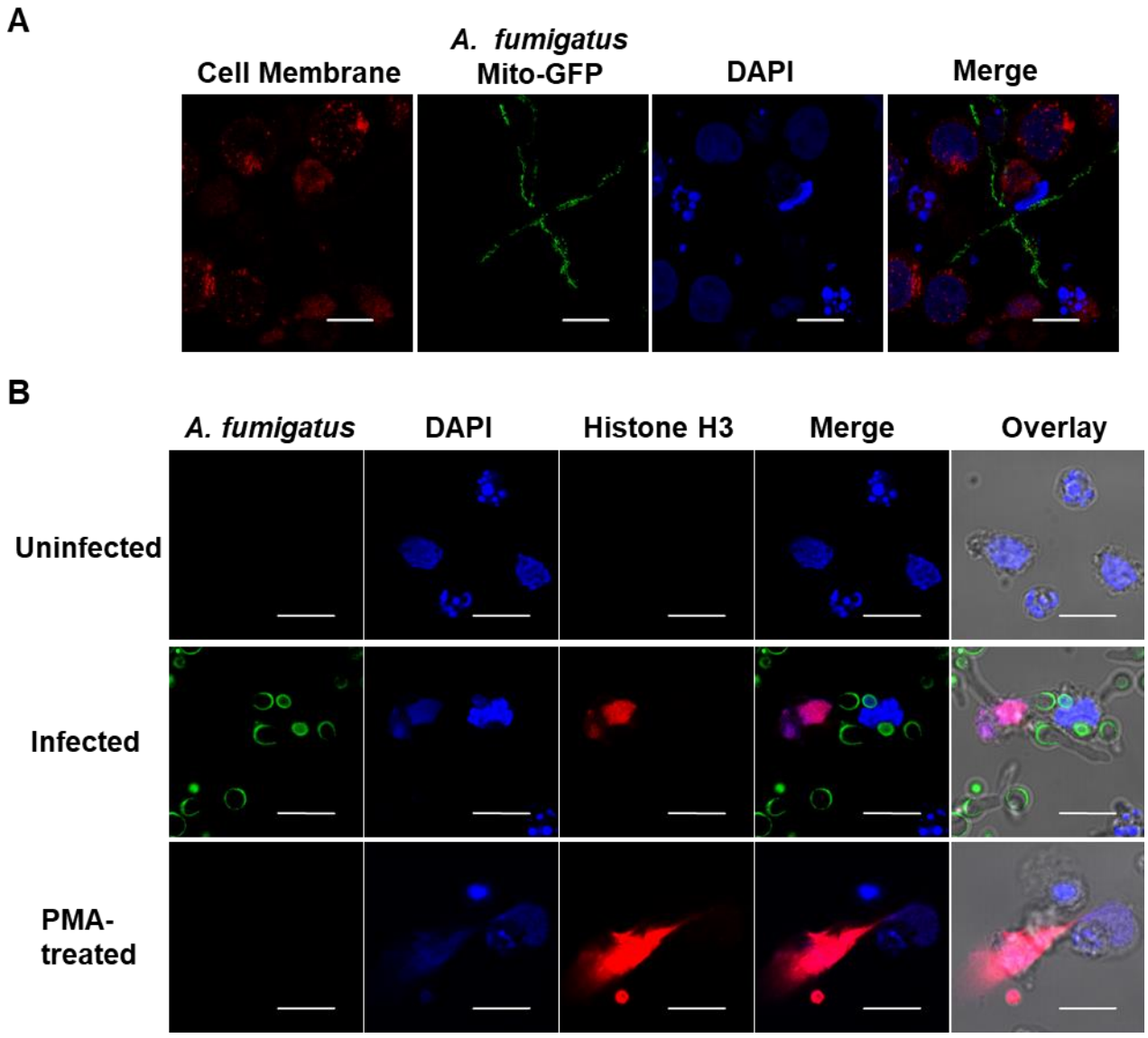

673

674 **FIG 3. Production of NETs in response to *A. fumigatus* infection**.

675 **(A)** Confocal scanning laser microscopy of nucleic acid stained with DAPI (blue) released from dPLB cells stained
676 with Cell Mask (red) after challenge with fungal hyphae containing a mitochondrial GFP reporter (*A. fumigatus*
677 strain AfS35 / pJW103 expressing a mitochondrial GFP reporter; green). Phorbol myristate acetate (PMA) was
678 used as a positive control. Data representative of three biological replicates. **(B)** Confocal micrographs of NET
679 markers, Histone H3 (red) and nucleic acid stained with DAPI (blue), produced by dPLB cells after contact with *A.*
680 *fumigatus* hyphae (FITC-labeled; green). Images are representative of three biological replicates. Scale bars are 10
681 µm.

682

683

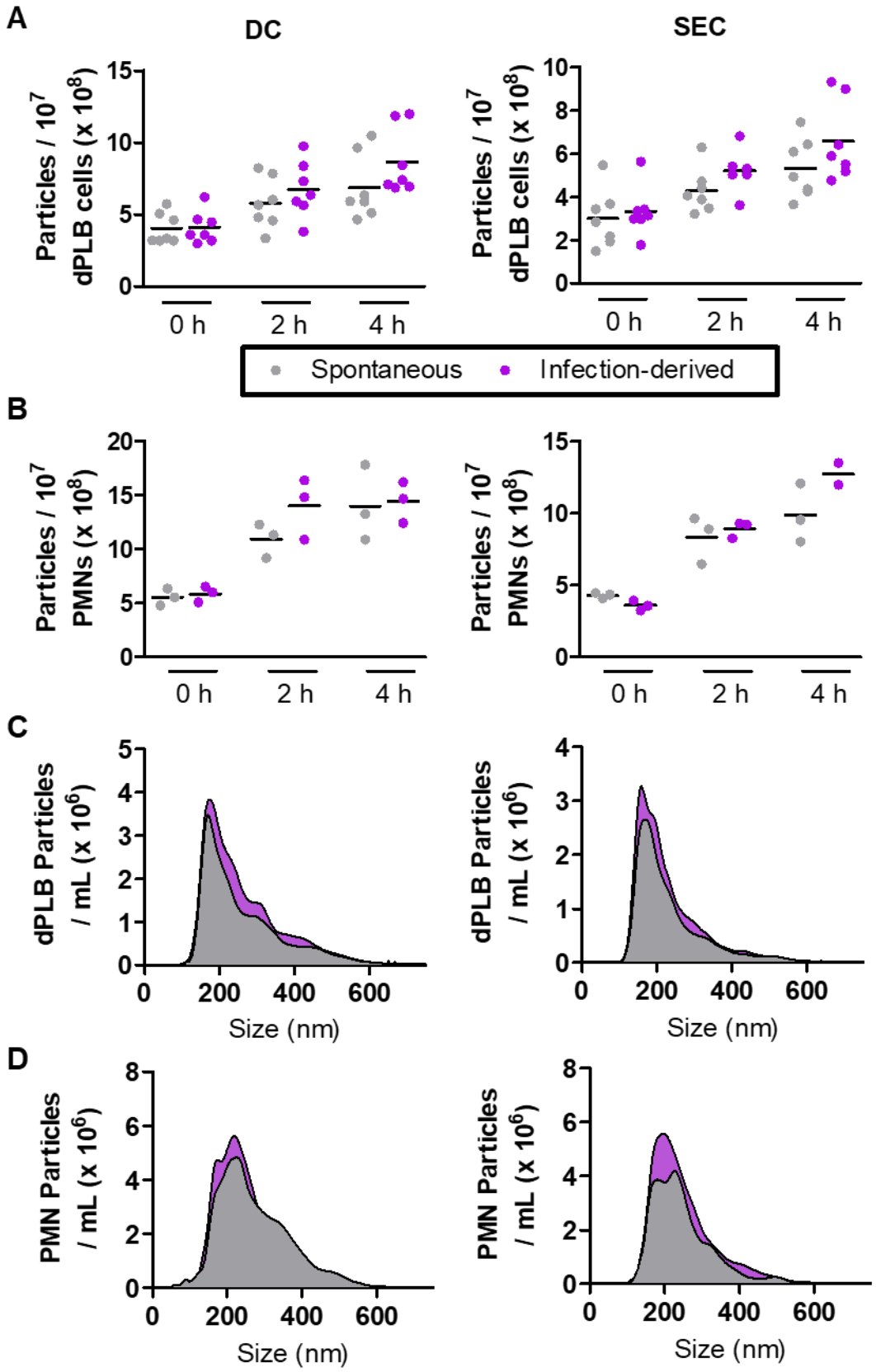

684

685 **FIG 4. dPLB cells produce extracellular vesicles comparable in size to primary human PMNs.**

686 Extracellular vesicles released spontaneously or produced in response to infection with opsonized *A. fumigatus*
687 conidia were isolated using a differential centrifugation-based approach (DC) or a size-exclusion chromatography-
688 based approach (SEC) and quantified using nanoparticle tracking analysis. Extracellular vesicles were quantified
689 from **(A)** dPLB cells or **(B)** primary human PMNs at 0, 2, and 4 hours post infection and show the average of six-to-
690 seven biological replicates and two-to-three biological replicates, respectively. Representative size histograms
691 from five biological replicates are shown for extracellular vesicles derived from **(C)** dPLB cells and **(D)** primary
692 human PMNs.

693

694

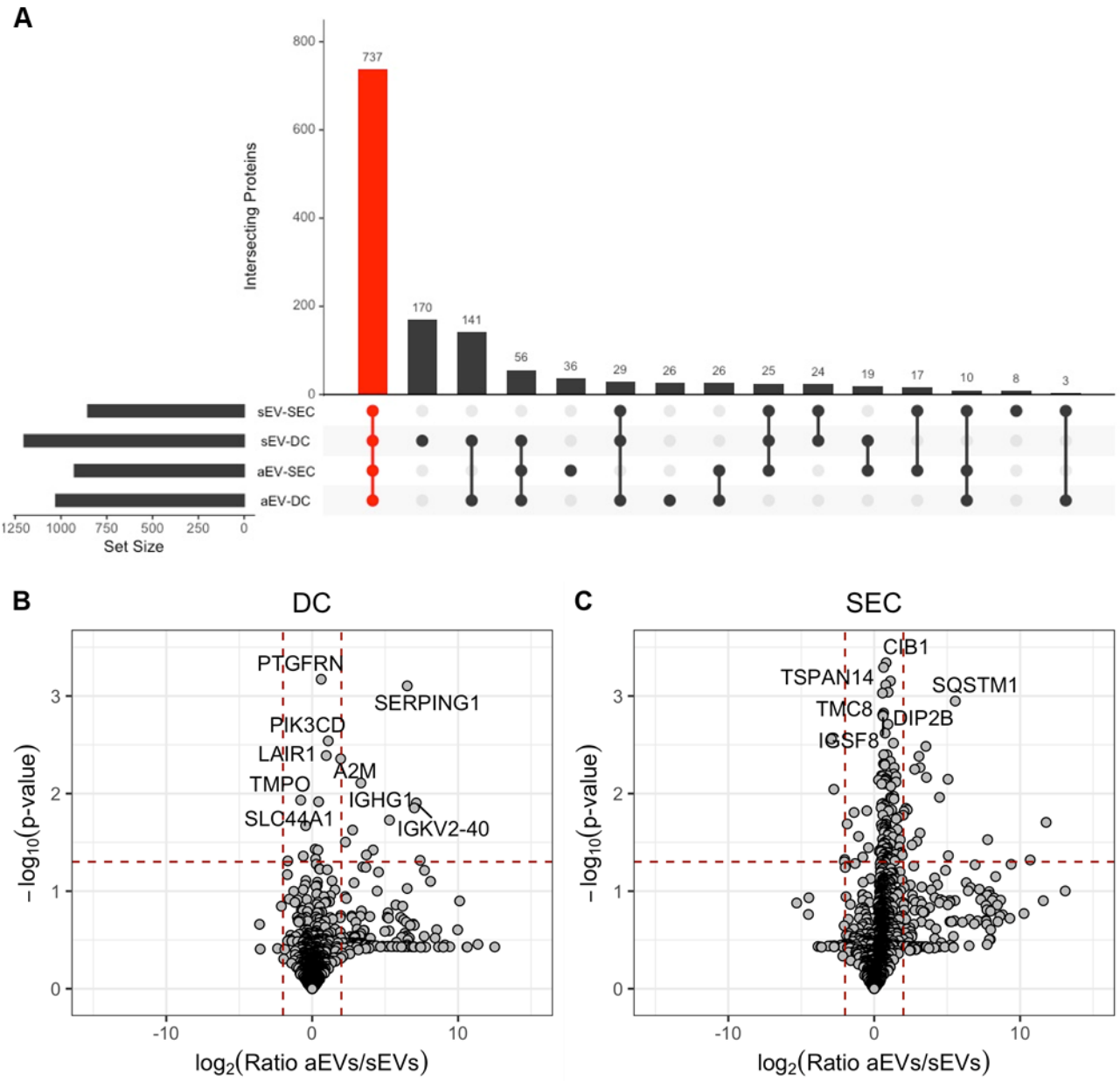

FIG 5. SEC enriches for extracellular vesicle populations.

LC-MS/MS proteomics analysis was performed on extracellular vesicles isolated from dPLB cells using a differential centrifugation-based approach (DC) or a size-exclusion chromatography-based approach (SEC) in the presence or absence of infection with opsonized *A. fumigatus* conidia. **(A)** Proteins identified in spontaneously released extracellular vesicles (sEVs) and infection-derived extracellular vesicles (aEVs) from at least two replicates of a given sample were intersected using UpSetR. The red bar indicates proteins that were found in all four samples. Volcano plots show the $\log_2$ ratio of infection-derived extracellular vesicles (aEVs) versus spontaneously released EVs (sEVs) for **(B)** DC-based isolation and **(C)** SEC-based isolation. Input data included values from all replicates

using the RMN data included in **Dataset S1**. Plots were created using ggplot2 in R. Proteomics data is from three analytical replicates of three independent biological replicates.

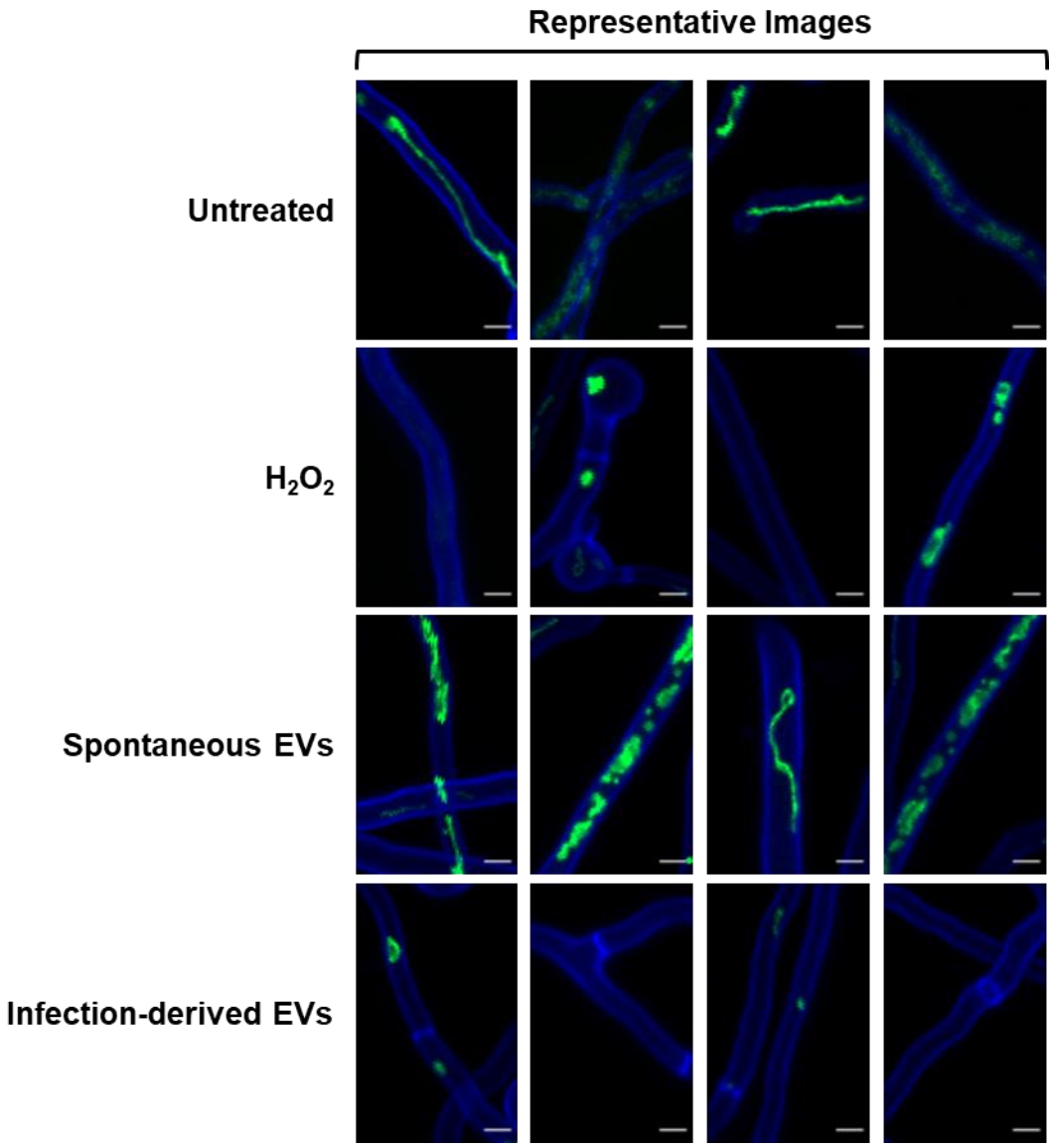

FIG 6. Infection-derived extracellular vesicles from dPLBs are antifungal to *A. fumigatus* hyphae.

A. fumigatus strain AfS35 containing plasmid pJW103 express a mitochondrial GFP reporter (green) were grown for 6 h and then stained with calcofluor white (blue) and incubated with spontaneously released extracellular vesicles or infection-derived extracellular vesicles overnight. As a control, untreated hyphae and hyphae treated with 3 mM H_2O_2 to induce cell death are included. An intact mitochondrial network is shown by a filamentous network, whereas a disrupted network is shown by fragmentation or the lack of green signal. Four example representative images are shown of each phenotype. Scale bars are 5 µm.

TABLES

Table 1. RMN-fold change of selected proteins identified in extracellular vesicles (EVs) from dPLB cells. Abbreviations: DC, differential centrifugation-based approach; SEC, size-exclusion chromatography-based approach.

Gene	Accession	Infection-derived EV (DC) / Spontaneous EV (DC)	Infection-derived EV (SEC) / Spontaneous EV (SEC)	Infection-derived EV (SEC) / Infection-derived EV-DC	Spontaneous EV (SEC) / Spontaneous EV (DC)
EV Markers					
CD63	F8VWK8	1.274	1.424	1.478	1.323
TSG101	F5H442	1.215	1.630	1.554	1.158
CD81	E9PRJ8	1.150	1.413	2.055	1.673
Non-EV Markers					
CANX (Calnexin)	P27824	-1.031	-1.082	-1.468	-1.398
MPO (Myeloperoxidase)	P05164	-1.024	1.026	2.063	1.963
CTSG (Cathepsin G)	P08311	1.045	1.042	1.117	1.120
AZU1 (Azurocidin)	P20160	-1.141	1.029	1.521	1.295